SMARTsurg

SMart we**A**rable **R**obotic **T**eleoperated **surg**ery

D5.3: Report on Haptic feedback system development

Due date: M18

Abstract: The present document is a deliverable of the SMARTsurg project, funded by the European Commission's Directorate-General for Research and Innovation (DG RTD), under its Horizon 2020 Research and innovation programme (H2020). This deliverable presents the preliminary results of Task T5.3 "Haptic feedback system development" obtained by M18 of the project. This is a preliminary version of the final deliverable that is due on M30. It is developed within the scope of WP5, responsible for Cognition and Dependability within SMARTsurg project. This deliverable outlines our current progress in the implementation of haptic feedback for suturing and palpation in a robot-assisted minimally invasive surgical scenario. Further, our preliminary investigations into sensorless force sensing for applications in a surgical situation are provided.

Dissemination Level		
PU	Public	x
PP	Restricted to other programme participants (including the Commission Services)	
RE	Restricted to a group specified by the consortium (including the Commission Services)	
CO	Confidential, only for members of the consortium (including the Commission Services)	

Document Status

Document Title	End user requirements, use cases and application scenarios
Version	0.6

D5.3: Report on Haptic feedback system development

Work Package	5
Deliverable #	D5.3
Prepared by	UWE
Contributors	UWE
Checked by	BUI, CERTH
Approved by	
Date	
Confidentiality	PU

D5.3: Report on Haptic feedback system development

Contact Points

Coordinator		
University of the West of England BRISTOL	University of the West of England Bristol Robotics Laboratory T Building, Frenchay Campus BS16 1QY Bristol UK	Tel: +44 117 32 81301 E-mail: Sanja.Dogramadzi@brl.ac.uk Website:http://www.brl.ac.uk/research/researchthemes/medicalrobotics.aspx

Partners		
CERTH CENTRE FOR RESEARCH & TECHNOLOGY HELLAS	Information Technologies Institute Building A - Office 1.1A 6th km Charilaou - Thermi, 57001 Thessaloniki, Greece	Tel.: +30 2311 257777 Fax: +30 2310 474128 E-mail: tzovaras@iti.gr Website: www.iti.gr/iti
POLITECNICO MILANO 1863	Building 32.2 Department of Electronics, Information and Bioengineering Via G.Ponzio 34/5 Milan, Italy	Tel.: +39 022 399 3371 E-mail: giancarlo.ferrigno@polimi.it Website: www.nearlab.polimi.it
Bristol Urological Institute	Brunel Building, Southmead Hospital BS10 5NB Bristol, UK	Tel.: +44 117 4140898 E-mail: anthony.koupparis@nbt.nhs.uk Website: www.nbt.nhs.uk/bristol-urological-institute
University of BRISTOL	Tyndall Avenue Senate House Department of Clinical Sciences BS8 1TH Bristol, UK	Tel.: +44 117 3423286 E-mail: r.ascione@bristol.ac.uk Website:http://www.bristol.ac.uk/health-sciences/research/tbrc/
IEO Istituto Europeo di Oncologia	Division of Urology Via Ripamonti, 435 20141 Milan, Italy	Tel.: +39 0257489516 E-mail: ottavio.decobelli@ieo.it Website: www.ieo.it
TheMIS THESSALONIKI MINIMALLY INVASIVE SURGERY ORTHOPAEDIC CENTER	TheMIS Orthopaedic Center 6 Adrianoupoleos St. 55133 Thessaloniki, Greece	Tel.: +30 2310 223 113 E-mail: papacostas@the-mis.gr Website: www.the-mis.gr/site/en
cybernetix A Technip Company	306 Rue Albert Einstein 13882 Marseille, France	Tel.: +33 (0)49121 7775 E-mail: jvandenbosch@cybernetix.fr Website: www.cybernetix.fr
Optinvent	R&D Department Avenue des Buttes de Coesmes 80 35700 Rennes, France	Tel.: +33 299871066 E-mail: khaled.sarayeddine@optinvent.com Website: www.optinvent.com

HIT HYPERTECH INNOVATIONS	HIT Hypertech Innovations 10 Polytechneiou Str. 3083, Límassol, Cyprus	E-mail: contact@hit-innovations.com Website: www.hit-innovations.com

Document Change Log

Each change or set of changes made to this document will result in an increment to the version number of the document. This change log records the process and identifies for each version number of the document the modification(s) which caused the version number to be incremented.

Change Log	Version	Date
First draft	0.1	June 22, 2018
Second draft	0.2	June 24, 2018
Third draft	0.3	June 24, 2018
Fourth draft	0.4	June 25, 2018
Fifth draft	0.5	June 25, 2018
Sixth draft	0.6	June 28, 2018

Executive Summary

The Task 5.3, as defined in the GA, has been set to investigate a haptic feedback scheme that can allow the surgeon to feel the forces applied to the surgical field. This includes kinaesthetic feedback (force or vibrations) acting on the surgeon through the exoskeleton. In this task haptic feedback provided through the Haption Virtuose 6D Desktop haptic device on the human arm and haptic feedback acting on the surgeon's hand while manipulating the soft tissue is analysed and compared. A Real-Time 3D software supervision will further be developed for the tele-operated system with the aim to effectively manage the force feedback (force measurement on the slave instrument side).

This task has been considered using the surgical requirements elicited in WP2 and reported in D2.1 and D2.2. The analysis of these documents identified the two most common tasks for which surgeons stated the need for haptic feedback – remote palpation of soft tissue and thread tension during suturing. The haptic feedback requires information supplied via remote force/pressure sensing between the tissue and the surgical instrument which has been developed in parallel to the haptic feedback system.

This document describes the methods and designs utilized to create sensing and haptic feedback systems and our preliminary test results. The force sensing and haptic feedback design studies are running in parallel and their integration and testing with surgeons are planned for the next 12 months.

D5.3: Report on Haptic feedback system development

Table of Contents

Contents

Executive Summary* .... *vi

1. Introduction* *9

1.1 Objective and Scope *9*

1.2 Document Structure *9*

1.3 Acronyms and Abbreviations *10*

2. Surgical haptic feedback* *11

2.1 Overview of haptic feedback in surgery *11*

2.2 Haptic feedback requirements for Smartsurg use cases *13*

2.3 Haptic feedback in urology – Suturing *13*

2.3.1 Use of the master device for suturing haptic feedback in Virtual Environment 14

2.3.2 Use of the master device for suturing haptic feedback in physical environments 15

2.4 Haptic feedback for Orthopaedics - Meniscus rupture detection *18*

2.4.1 Device design and functionality 18

2.4.2 Preliminary user testing 21

2.4.3 Path Following and Identification of object hardness in virtual environment 25

3. Force sensing for haptics in RAMIS* *28

3.1 Sensor-less force sensing *28*

3.1.1 Experimental Setup 28

3.1.2 Preliminary results 29

3.1.3 Discussion and future work 30

3.2 Force sensing for suturing task *31*

4. Conclusion and future work* *31

Appendices* *32

Appendix A: Haption Virtuose 6D Desktop Datasheet *32*

Appendix B: KUKA IIWA Datasheet *34*

Appendix C: Phantom CAD drawings *35*

References* *42

1. Introduction

1.1 Objective and Scope

This deliverable (D 5.3 – “Report on Haptic feedback system development”) reports the Smartsurg project progress on the development of haptic feedback for different surgical use case studies. Haptic feedback requirements have been elicited in the first stage of the project and reported in D2.1 and D2.2. As part of haptic feedback requirements, we are also reporting on force sensing strategies involved in surgical tasks.

Particularly this document outlines:

- Surgical use cases that benefit from haptic feedback
- Sensing in surgical environment
- Haptic feedback design and implementation
- Preliminary results
- Conclusion and future work

1.2 Document Structure

The document starts with a brief overview of haptic feedback in surgery followed by the surgical requirements elicited in the first 8 months of SMARTsurg project which formed the basis of all subsequent development. Section 2 details our method of development of haptic feedback design for two selected surgical tasks. Section 3 presents our work on force sensing for haptic feedback with two different force sensing methods that correspond to two haptic feedback systems. Section 4 presents conclusions from our current work and what is planned for the next 12 months.

1.3 Acronyms and Abbreviations

Abbreviation	Definition
RAMIS	Robot assisted minimally invasive surgery (or surgical)
MIS	Minimally invasive surgery
RMS	Root mean square
FHD	Fingertip haptic device
DOF	Degrees-of-freedom

2. Surgical haptic feedback

2.1 Overview of haptic feedback in surgery

Robot-assisted minimally invasive surgery (RAMIS) through use of the da Vinci master-slave surgical system offers improved vision, precision and patient recovery time compared to traditional laparoscopic surgery. However, certain shortcomings prevent RAMIS from fulfilling its maximum potential, including the lack of haptic feedback provided to the surgeon [1]. One of the Smartsurg project objectives is to investigate the requirements for haptic feedback in 3 different surgical areas. A full scope of this investigation is reported in D2.1.

Minimally invasive surgery (MIS) and RAMIS is conducted by making small incisions on the abdomen of the patient. Trocars are placed through the incisions and long laparoscopic surgical tools and an endoscope placed inside the trocars to access the surgical site. In traditional open surgery, the surgeon would directly manipulate organs with their hands and thus be provided with haptic feedback. This feedback is lost in RAMIS as the surgeon manipulates the surgical site remotely via a master-slave, which apply forces on the organs. As such, surgeons have no knowledge of the amount of force they are applying to tissues and organs, and could cause irreversible trauma.

Ethical and technical issues preclude data on forces exerted by laparoscopic tools during operations on humans from being measured. Nevertheless, in-vivo experiments measuring applied forces in manual MIS situations have been conducted in animal trials. Yamanaka et al. [2] performed a laparoscopic nephrectomy in an in-vivo porcine experiment. From four tests, they found an overall maximum grasping and pulling forces of 42 N and 9 N, respectively. The grasping and pulling forces they found to tear off various organs are tabulated in Table 1. In a similar study, Barrie et al. [3] performed in-vivo porcine experiments to determine grasping forces encountered in manual MIS for various abdominal organs. From grasping trials conducted on five abdominal organs (five trials each), they found an overall maximum grasping force of 75 N which was achieved by grasping the colon. The mean maximum and root mean square (RMS) grasping forces they applied to abdominal organs are tabulated in Table 2. Based off results in their earlier work, Barrie et al. [4] investigated safe grasping thresholds in laparoscopic colorectal surgery. Forces from 10 to 70 N were applied to a porcine colon in-vivo, for three grasping durations of 5, 30 and 60 s. It was found that significant histological differences (i.e. irreversible trauma) between grasped and ungrasped regions of the colon existed when upwards of 50 N was applied, irrespective of the duration. Whilst these trials were conducted using manual MIS techniques and investigated maximum capabilities of surgical tools, the results of these works are extremely relevant for RAMIS and indicate the importance of supplying surgeons with haptic feedback to reduce applied force on tissue and minimise the risk of causing irreversible trauma.

Table 1: Forces required to tear off organs in partial nephrectomy [2]

Organ	Grasp Force [N]	Pull Force [N]
Liver	26	9
Kidney	12	4
Renal vein	15-20	2
Gonadal vein	8-15	3

Table 2: Grasping force applied to abdominal organs [3]

Organ	Mean Max Force [N]	Mean RMS Force [N]
Colon	59	24.6
Gallbladder	50.7	24.3
Rectum	49	21.4
Bladder	28	21.9
Small bowel	22.4	9.7

Investigations have been conducted into the benefit of haptic feedback (tactile and force) in RAMIS. Tactile feedback was implemented in a da Vinci Surgical System and applied grasping forces and consequent tissue damage in a ‘run the bowel’ experiment evaluated [5]. It was found that when tactile feedback was activated, median grasping force of the dominant and non-dominant hand of novice subjects decreased from 3.5 N to 2.3 N and 3.7 N to 2.7 N respectively; and for expert subjects median applied force decreased from 3.8 N to 2.2 N and 2.8 N to 2.0 N for the dominant and non-dominant hands respectively. Furthermore, tissue damage was reduced when tactile feedback was provided. The impact that haptic feedback has in a palpation task has also been investigated [6]. Slices of porcine organ were palpated using a haptic grasper in a box trainer setup in which participants were blinded. Haptic feedback reduced the average applied palpation force from 4.6 N to 1.7 N. Similarly, Talasaz and Patel [7] and Gwilliam et al. [8] found improved performance in palpation tasks when haptic feedback was provided to the user.

Suturing is another area where haptics in RAMIS would be beneficial as excessive suture breakage is a major problem encountered by both skilled and novice surgeons [9]. Force levels in a hand tied suture (i.e. participant has natural force and tactile feedback), instrument tied suture with force feedback and a suture performed with the da Vinci robot without any feedback has been investigated [9,10]. The authors demonstrated that the instrument tied suture corresponded best to the hand tied suture and that the addition of haptic feedback would be beneficial for RAMIS performed sutures. Furthermore, other studies into the role of haptic feedback in RAMIS for suturing have been performed providing similar conclusions; the addition of haptic and visual feedback is beneficial for RAMIS in a suturing context as forces applied to the sutures is reduced leading to fewer breakages [11, 12].

This review has shown that the addition of haptic feedback to RAMIS is beneficial as applied forces on tissue are reduced, and therefore the risk of irreversible tissue trauma. Furthermore, the use of haptic feedback in suturing tasks has been shown to reduce applied forces to sutures, resulting in fewer breakages. However, whilst it is clear that haptic feedback will be beneficial in RAMIS, the challenge in successful implementation is the sensing of forces at the surgical site given the restrictions imposed. Potential solutions to this are the focus of Section 3 of this deliverable.

2.2 Haptic feedback requirements for Smartsurg use cases

Haptic feedback requirements have been established by the many surgeons involved in Smartsurg survey in WP2. Their answers have been extracted and analysed prior to defining functional and non-functional requirements for the design of sensing and haptic feedback devices. The most frequent opinions are summarised here.

Orthopaedic soft tissue surgeons:
O1: Lack of the soft tissue feel
O2: Lack of the ability to verify the tissue hardness/thickness
O3: Lack of the ability to palpate/probe meniscus rupture (feel what the endoscopic camera cannot see)

Urologists:
U1: Lack of tactile feedback during cutting and suturing
U2: Lack of feel during tissue pushing/pulling
U3: Lack of haptic feedback during organ retraction

Cardio surgeons:
C1: The surgeon needs to feel the tissue quality
C2: Lack of the feedback whilst suturing

We have grouped these responses into two haptic development tasks:
1. Suturing (thread tension) sensing and haptic feedback; and
2. Palpation/Probing sensing and haptic feedback
The palpation haptic feedback is being developed for the orthopaedic case study and will be demonstrated in meniscus rupture palpation.
The suturing feedback is common to all these surgical areas and will be demonstrated in a suturing task in the urology case study.

2.3 Haptic feedback in urology – Suturing

Suturing during minimally invasive surgery is one of the most challenging and time consuming of all surgical subtasks [13]. Using an endoscope alone makes it challenging for surgeons to estimate angles and distances and extracting a needle from tissue at a desired point often requires several attempts. This extends the operating time but also causes trauma to the surrounding tissue which can further add to the operating time if tissue repair is needed [14]. Attempting to move a laparoscopic instrument while watching a 2D, or even a 3D, video monitor is somewhat counterintuitive especially where users are required to estimate forces exerted on tissue from the pressure applied by surgical tools based solely on visual information provided by a 2D/3D video. This is not only difficult and error prone, but it is also not possible to see the surgical area from multiple viewpoints and thus, some points where tools are exerting pressure may not be noticed, resulting in tissue trauma.

Tasks such as suturing could benefit from haptic feedback since this could enhance the capabilities of junior surgeons and save valuable time during an operation, for example if breaking of a suture or causing bleeding due to excessive pulling of the suture is avoided.

The predominant movement and subsequent tension in a suturing manoeuvre is created by and felt in the surgeon's wrist. With respect to the overall master device setup (i.e. exoskeleton and Virtuose 6D Desktop), wrist motion of the surgical instrument is to be controlled via the Virtuose 6D Desktop device. As such, the thread pulling forces encountered in a suturing task with the SMARTsurg system are to be reflected on the Haption device.

The process of implementing haptic feedback on the master Virtuose 6D Desktop device for suturing in a physical environment is categorised into three stages:

Stage 1: detecting forces that a shaft applies on a static object and reflecting the forces on the master device

Stage 2: detecting forces that a shaft applies to a trocar whilst conducting a suturing task and reflecting the forces on the master device

Stage 3: estimation of shaft forces from a load cell attached to the KUKA flange and reflecting the forces on the master device

2.3.1 Use of the master device for suturing haptic feedback in Virtual Environment

The aim of this task is to investigate the use of haptic feedback during suturing, specifically focused on pulling the thread while tying a knot. The master instrument (Virtuose 6D Desktop) interacts with a simulated surgical environment that depicts a thread suturing the tissue and modelled thread/tissue tension forces. A virtual needle's position is controlled by the Virtuose 6D Desktop which provides corresponding tension force feedback to the user.

Figure 2.1 depicts a suturing task simulated in the virtual envirnoment CHAI 3D which has been interfaced with the Virtuose. In addition, and as a comparison, the open-source surgical simulation framework OpenSurgSim will be explored [15].

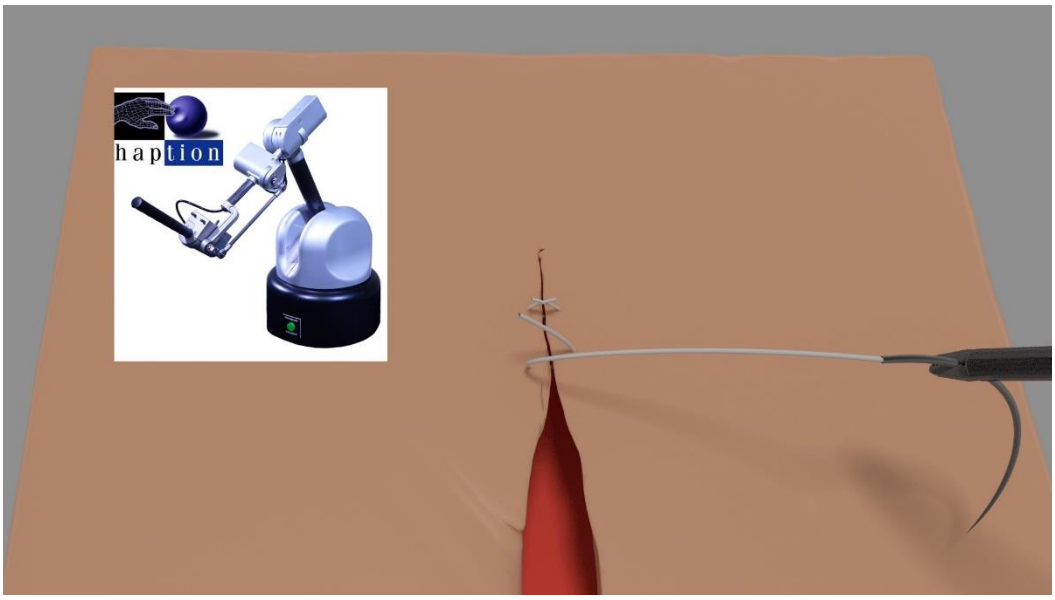

Figure 2.1: Virtual suturing task; the needle holder is controlled via Virtuose 6D Desktop

Initial user studies will be conducted where participants will grasp the virtual needle using the master device and pull it as much as they believe should be enough to tie a hypothetical knot. The more the participant pulls, the more tension on the thread will be present (resistance from the master). The maximum pulling force will be recorded. The task will be acompanied with visual cues indicating the thread tension: the two tissue sections will either get closer or further apart and deform when the thread is pulled too much and finally, the thread or tissue will tear if the thread is pulled beyond a limit (at this point, the haptic feedback force is removed).

Different trials will involve different levels of force feedback. It will be recorded how much above the optimal force magnitude, defined for each test, the participant will stop pulling the virtual thread.

These tests will be based on testing real surgical sutures using a load cell and measuring the required thread tension when creating a surgical knot and forces that tear the thread. The results of the virtual haptic interface experiments will inform how these forces should be modelled in the master device for implementation of haptic feedback in a real environment.

2.3.2 **Use of the master device for suturing haptic feedback in physical environments**

2.3.2.1 Experimental setup

The three stages of haptic implementation utilise a bilateral master-slave teleoperation scheme. The master device (Virtuose 6D Desktop) controls the position of the slave device (KUKA IIWA) and the force interaction the slave experiences reflected back to the master. The force the master reflects to the user is to be measured via a load cell. The concept of the bilateral teleoperation scheme is illustrated in Fig. 2.2.

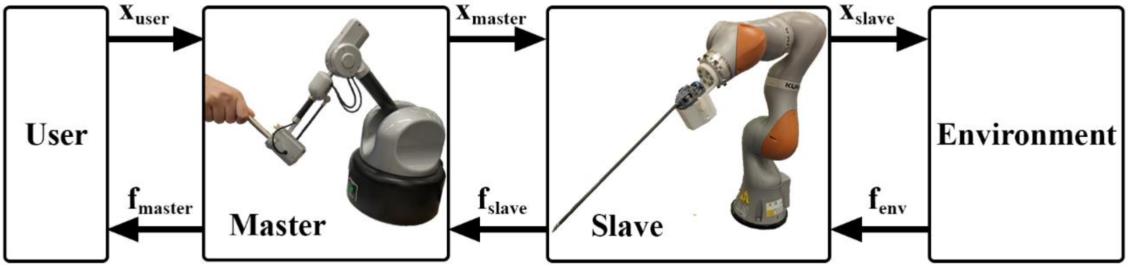

Figure 2.2: The bilateral teleoperation scheme employed by the SMARTsurg system

Stages 1 and 2 of the haptic testing utilise a da Vinci endoWrist surgical tool. This tool is mounted to the flange of the KUKA arm via a custom housing as shown in Fig. 2.3. Stage 3 of the experiments will be conducted with a three fingered surgical instrument prototype that is attached to the KUKA flange in a similar manner to Fig. 2.3.

Figure 2.3: Custom housing that interfaces with da Vinci endoWrist tools and mounts onto the KUKA flange

Stage 1

Stage 1 is used for verification of the bilateral teleoperation between the master and slave. In this experiment, the shaft of the da Vinci endoWrist tool is impacted against a soft vertical wall, as shown in Fig. 2.4. A SingleTact 0-10 N measurement range force sensor is attached to the shaft to measure the magnitude of the contact force. This force is reflected back to the user via the master device.

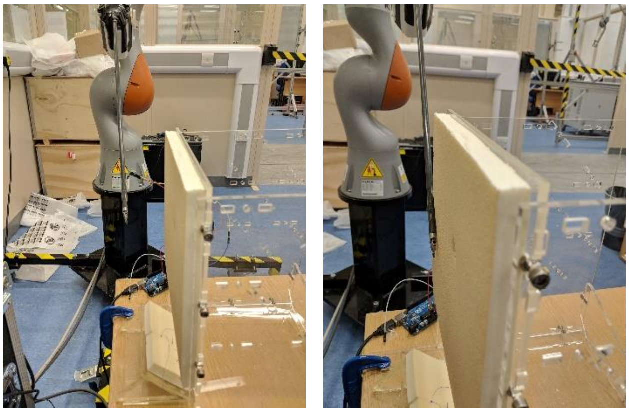

Figure 2.4: The slave arm in the home position (left) and impacting the soft wall (right) for stage 1 experiments

Stage 2

Stage 2 of the experimental testing mimics a minimally invasive suturing scenario. In this experiment, a trocar is penetrated through the artificial skin with the shaft of the surgical instrument (a needle driver) passing through the trocar. The jaws of the needle driver hold a suture, with the jaws held firmly in place via locking cogs in the housing that attaches to the KUKA flange. An organ is replicated by a foam pad on which a suturing task is to be performed using the master-slave system. The forces that the shaft exerts on the trocar during the performed task are measured by two SingleTact forces that are mounted inside the trocar, with these forces reflected to the master device.

Stage 3

The experiments in stage 3 will be conducted using a three fingered surgical instrument prototype. The experimental setup will be similar to stage 2; however, instead of the foam pad a phantom kidney will be utilised. Further, the forces exerted by the shaft whilst suturing will be estimated by a load cell mounted on the KUKA flange. The shaft forces will then be estimated from the measured flange forces and reflected to the user via the master device.

2.3.2.2 Preliminary results

Stage 1

In this stage the operator is teleoperating the slave arm by holding and moving the end-effector of the master device. The motion of the end-effector of the master arm in the Cartesian space is directly mapped to the motion of the end-point of the instrument that is attached on the slave arm. The preliminary results of the experiment are shown in Fig. 2.5, 2.6. The operator moves the master device so that the slave arm moves the instrument shaft in the y direction towards the soft wall. When the instrument comes into contact with the wall ($t = 9 - 12s$ in Fig. 2.5, 2.6), the force measured by the SingleTact sensor (Figure 2.6) is fed back to the master device. The sudden force feedback causes the operator to slightly recede to the opposite direction (detail at $t = 9s$, Fig. 2.5) whereas the slave arm, having detected a collision stops its motion temporarily. After that, the operator teleoperates the instrument shaft away from the soft wall. Fig. 2.5 shows the y-component of the relative positions of both the master and slave arm with respect to their initial positions. The delay between the master and slave arm is caused by the current teleoperation scheme and will be minimised in later versions. Fig. 2.6 shows the force that is measured on the shaft in the y direction which is proportionally applied to the master device.

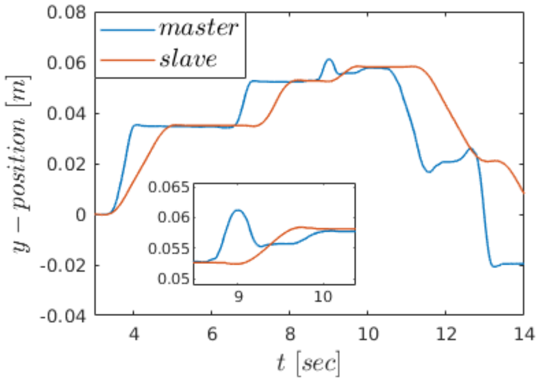

Figure 2.5: y-component of the relative master/slave position

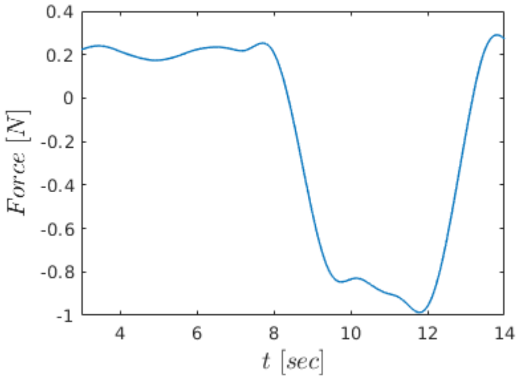

Figure 2.6: Force measured by a SingleTact sensor and applied to the master device

2.4 Haptic feedback for Orthopaedics - Meniscus rupture detection

Orthopaedic surgeons often have to assess if and how much the meniscus has been damaged during arthroscopy. Due to its position at the back of the knee, parts of the meniscus cannot be inspected using the inserted endoscopic camera. In the discussions with the surgeons, it was proposed to develop a palpation mechanism that can access the meniscus and a haptic device that can provide the palpation sensation to the surgeon. We have developed a Fingertip Haptic Device (FHD) that provides cutaneous haptic feedback to the user about the hardness and compliance of the remote object (in this case the meniscus being palpated). The FHD is 3D printed and comprises a soft fingertip platform of adjustable compliance which is linearly actuated in respect to the fingertip. The device design and functionality has been published in Frontiers in Robotics and AI, Special Issue on Innovative Haptic Interfaces Emerging from Soft Robotics (‘Design of a Wearable Fingertip Haptic Device for Remote Palpation: Characterisation and Interface with a Virtual Environment’) [16].

2.4.1 Device design and functionality

Figure 2.7 shows the side and front view of the FHD, which consists of: (a) the Variable Compliance Platform (VCP), (b) the Rack and Pinion (RP) mechanism and (c) the Support Structure (SS) with the IMU sensor. The RP mechanism adjusts the distance between the fingertip and the VCP. The FHD’s dimensions are 38.6 mm (width) x [38.2–53] mm (variable length due to the RP). The distance between the SS and the VCP range from 9.6 to 24.53 mm. The total weight of the FHD (including one motor, TowerPro MG92B) is 40 gr.

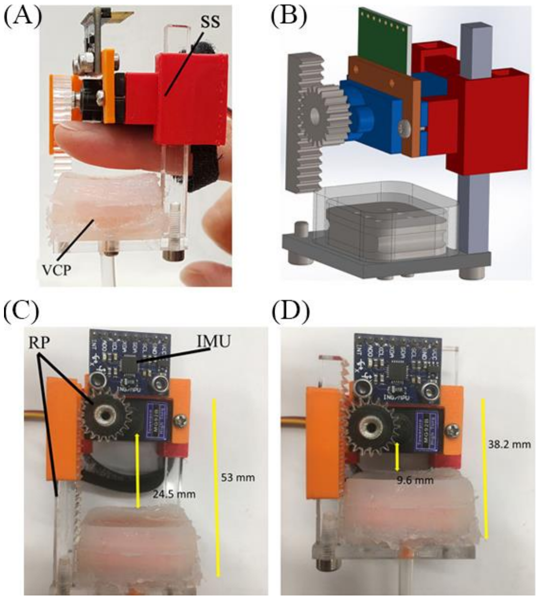

Figure 2.7: FHD components

The 3D printed (Polylactic Acid filament) VCP has an area of 478.5 mm^2 that corresponds to the average area of a fingertip as reported by Peters et al. [17] (index finger, female average 360 mm^2, male average 420 mm^2).

Fingertip haptic feedback is often achieved by pressing rigid [18,19,20] or soft (e.g., belt systems by Minamizawa et al. [21]; Pacchierotti et al. [22], dielectric elastomer actuators by Koo et al. [23], Frediani et al. [24]) objects either normal or lateral to the fingertip surface. However, these devices do not offer actual indentation sense because their compliance cannot be changed. Our hypothesis is that variable compliance in a haptic device can provide indentation and varied hardness/softness sense to the user. Consequently, the VCP consists of a rigid base (Fig. 2.8) with its top surface covered by a layer of silicon rubber (DragonSkin, shore hardness 10 A, 475 psi) of 1 mm thickness. The lower surface (Fig. 2.8A) of the VCP is connected to a syringe pump via a 7 mm diameter air tube (Fig. 2.9). The VCP functionality is created by pumping air through 6 holes (Fig. 2.8B) into the gap between its rigid base and the soft silicon membrane of the VCP.

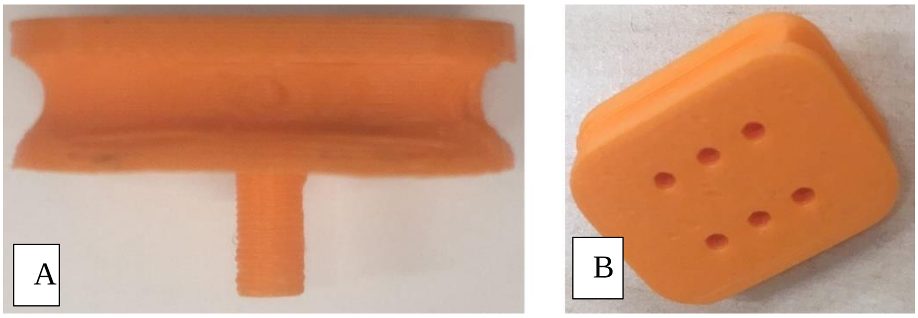

Figure 2.8: 3D printed base of the VCP

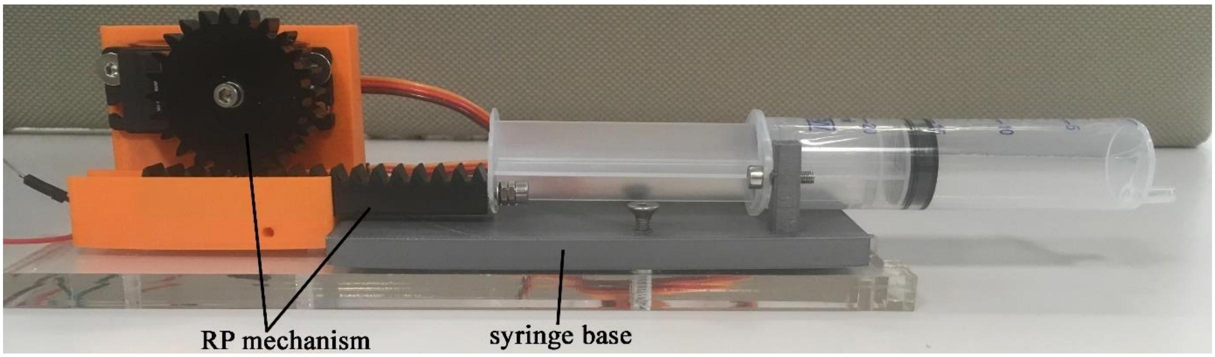

Figure 2.9: Rack and Pinion mechanism and the syringe that supplies air to the VCP

The design of the syringe pump actuation system, shown in Fig. 2.9 utilises an RP mechanism (part 1, Fig. 2.9) and a 20 ml syringe (attached to part 2, Fig. 2.9). The pinion is attached to a motor (Turnigy 1258 TG, stall torque of 1.17 Nm) and the rack moves the syringe along the horizontal axis (0.8 mm displacement per one degree of rotation). The maximum volume of air used for inflation of the VCP was 4 ml, equivalent to pressure of 5.17 kPa, measured using a pressure sensor (HSCSAAN015PDAA5, Honeywell, USA, range of ±103 kPa, accuracy of 0.25 kPa).

The extent of the VCP's deformation when inflated with 4 ml of air is 25 mm, while index fingertip extent is 10.4 mm in average for women and 12.7 mm for men [17]. The extent of the VCP is greater than the measured human fingertip because the contact area will be smaller when the soft membrane is inflated.

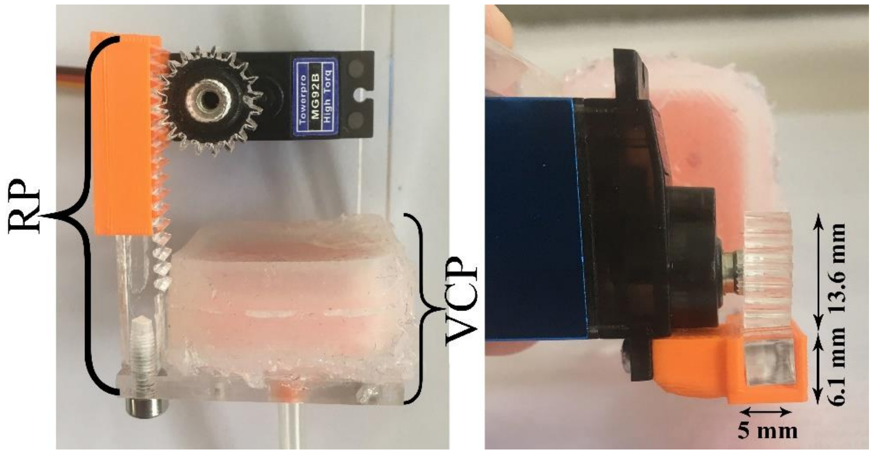

Figure 2.10: The RP mechanism and its dimensions

The chosen mechanism provides linear displacement of the VCP towards the fingertip and control of the indentation of the inflated membrane. The rack length is 30 mm (other dimensions are shown in Fig. 2.10). This design was preferred to a parallel mechanism [19, 22] to keep the size of the FHD to the minimum.

The shaft of the motor (TowerPro MG92B, stall torque of 0.3 Nm) is directly attached to the pinion. The linear displacement δ of the VCP can be calculated as follows:

$$\delta = 2\pi \frac{d}{2} \frac{\theta}{360} \quad (1)$$

where θ is the angle of motor rotation and d is the diameter of the pinion. Due to the required teeth precision, both rack and pinion were laser-cut in acrylic.

The variable compliance is created by varying the pressure inside the VCP which is a function of the piston movement (x) and the movement of the RP (h). It can be approximated using (2):

$$p = p_0 + k_p(x + h) \quad (2)$$

where p is the pressure inside the VCP, p_0 is the initial pressure, k_p is the air spring constant between the piston and the finger. The piston movement (x) is proportional to the air volume supply through the syringe. The perceived hardness will be tested by a range of combinations of x and h that will effectively create different indentations in the human finger.

2.4.2 Preliminary user testing

In order to represent and assess how hard the FHD is, a wider user study was carried out with 15 participants (18–34 years old, ratio of women/men 7/8, ratio of right/left dominant hand 13/2). The participants were asked to put the FHD on their dominant hand's index fingertip and score the hardness of the touch on a scale of 1–5 (hard to soft). The experiments tested 10 different conditions created by varying the air volume inside the VCP as well as its linear displacement (and proximity to the fingertip). In one of the conditions, the VCP was not inflated while its linear displacement was 5.72 mm. The remaining 9 combinations are presented in Table 3. In this Table, "x" means that for that specific volume of air, the level of pressure could not be achieved. Each condition was tested 5 times by each participant in a randomised order after a short "training" session in which the participants could experience the different hardness levels of the FHD.

Table 3

		Air volume in the VCP		
		2 ml	3 ml	4 ml
Resulting	3.5 kPa	1.1 (5.2 mm)	1.2 (2.08 mm)	X
Pressure	4.5 kPa	2.1 (7.28 mm)	2.2 (5.2 mm)	X
	5 kPa	3.1 (7.8 mm)	3.2 (5.72 mm)	3.3 (2.08 mm)
	7 kPa	X	4.2 (8.32 mm)	4.3 (6.76 mm)

These experiments have compared the hardness perception of different users for the same level of pressure at different volumes of air in the VCP. For example, 3.5 kPa can be derived at 2 ml of air and 5.2 mm displacement as well as at 3 ml of air and 2.08 mm displacement of the VCP. The experimental measurements that were used are the ones presented for the male participant of the previous experiment presented in Fig. 2.9. Code names for each combination of air pressure and volume in the VCP that was used in this study, as well as the measured normal force exerted (micro load cell CZL635, Phidgets), are shown in Table 4.

Table 4

Condition	Normal Force [N]	Code in Table 4	Air Volume in VCP [ml]	Resulting Pressure [kPa]
1	6.23	3.1	2	5
2	2.87	2.2	3	4.5
3	4.33	4.3	4	7
4	5.55	2.1	2	4.5
5	3.14	1.1	2	3.5
6	6.76		No air	
7	7.31	4.2	3	7
8	1.68	3.3	4	5
9	0.93	1.2	3	3.5
10	3.14	3.2	3	5

The box graph of Fig. 2.10 illustrates how participants scored the hardness of the VCP for each condition. While the hardness of condition 6 (the VCP was not inflated) was evaluated with a score of "1" (hard), conditions 8 (4 ml of air) and 9 (3 ml of air) were evaluated as the softest (scores of "4" and "5"). In both conditions, the VCP moved by 2.08 mm and applied force to the fingertip of participants gently with the percentage of hardness score "4" and "5" being similar; however, the percentage of score "5" is higher in condition 9 (just above 35%), which suggests that for the same displacement, the VCP feels softer when filled with 3 ml of air. At 3 ml, the VCP is at medium capacity which makes it more compliant than at 2 ml or 4 ml. This is also seen when comparing conditions 2 (3 ml of air) and 5 (2 ml of air), for which the percentage of score “2” is under 20% and just above 35% respectively and hence condition 2 is considered softer.

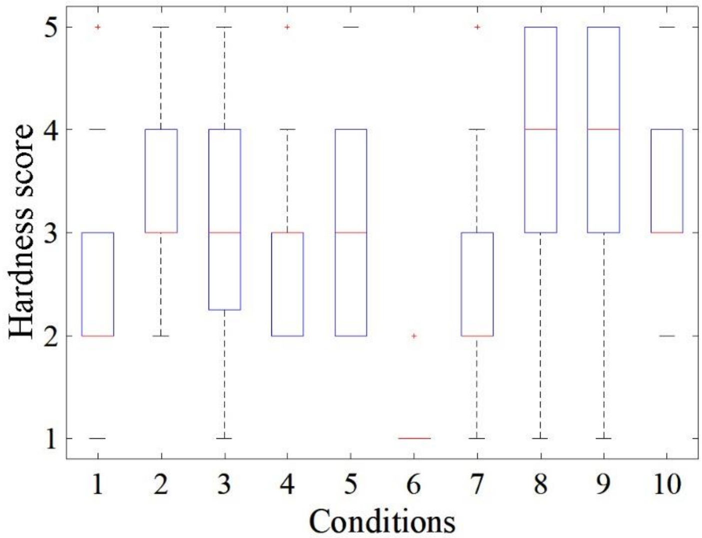

Figure 2.10: Participants perception of hardness for different conditions

The distribution of hardness score for conditions 1, 4 and 7 was between “2” and “3”. The percentage of score “2” of condition 1, 4 and 7 was approximately 50, 40 and 49% respectively, with condition 4 providing slightly softer feeling than conditions 1 and 7. This was expected as the VCP was displaced by 0.52 mm more (1 step) than in condition 4. A comparison between conditions 1 and 7 shows that in the latter, the VCP has 1 ml of air more and it is displaced by 1 step more than in condition 1. As the hardness score is similar for these conditions, this indicates that 1 step of increase in air volume cancels out 1 step of increase in displacement. Comparing conditions 5 (2 ml of air) and 3 (4 ml of air and 3 steps of displacement more than condition (5), their percentage of the combined score of “3” and “4” is similar. However, condition 5 had a more equal distribution between scores “2”, “3” and “4” than condition 3 which, as will be discussed later, prompted a more consistent response between participants. For conditions 2 and 10, the distribution was similar due to only 1 step of displacement difference between them, mainly between scores “3” and “4”, with “3” being the prevailing score. However, conditions 3 and 10 seem to have a clearer tendency towards a score of “3”, with condition 10 (3 ml of air) considered slightly softer. Finally, Fig. 2.9 shows that there was no significant difference between responses of men and women, with SD for conditions 1–10 respectively: 0.07, 0.11, 0.17, 0.15, 0.1, 0.04, 0.13, 0.14, 0.27, 0.11 (mean of 0.128).

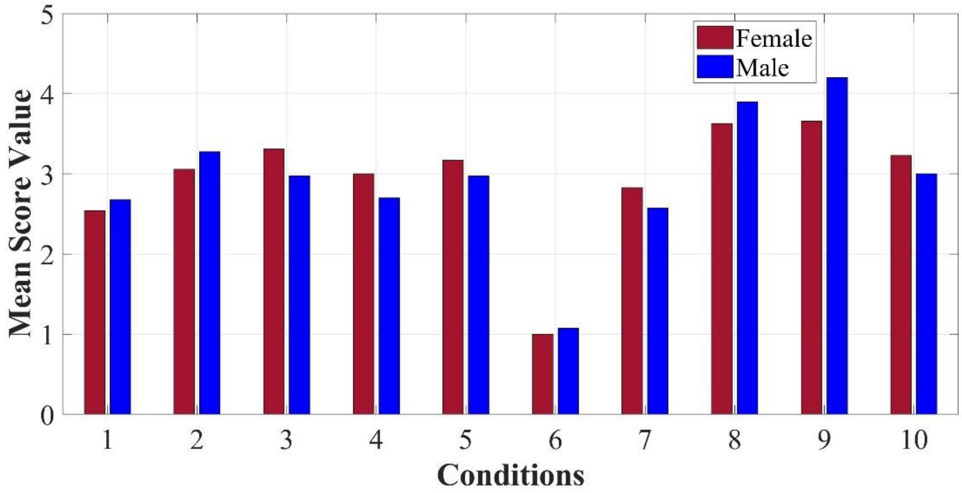

Figure 2.11: Mean scores for responses of women (red colour) and men (blue colour)

It is worth noting that user perception of hardness does not always correlate with the measured normal force exerted by the VCP. For example, condition 7 was considered softer than 6 despite the VCP exerting higher normal force in the former. This is due to the inflation of the VCP with 3 ml of air.

The 2nd column of Table 5 summarises the conditions that correspond to each score of the 1st column according to most of the participants' answers. However, for conditions 1 and 10, the participants' responses were not consistent (each condition was randomly repeated 5 times). For example, participant A scored condition 1 with "2, "3", "4", "2", "3" across the 5 repetitions of the test, while participant B scored condition 5 with "2","3", "3", "2", "2". This would indicate that condition 5 receives more robust (consistent) responses than condition 1, as the participant appoints the same score to it more times (in this case, score "2" and "3", instead of score "2", "3" and "4"). Based on this criterion, conditions 2, 5, 6, 8 and 9 were the most robust, as shown in the 3rd column of Table 5. Figure 2.12 shows the distribution of the "robustness percentage" of all conditions, determined by whether a participant's set of (5) responses regarding a condition contained a maximum of 2 different scores (e.g., "2" and "3").

Table 5

Score (1-5, hard-soft)	Condition with highest percentage	Conditions with consistent responses
"1"	6	6
"2"	1	5
"3"	10	2
"4"	8	8
"5"	9	9

It is worth noting that user perception of hardness does not always correlate with the measured normal force exerted by the VCP. For example, condition 7 was considered softer than 6 despite the VCP exerting higher normal force in the former. This is due to the inflation of the VCP with 3 ml of air.

The 2nd column of Table 5 summarises the conditions that correspond to each score of the 1st column according to most of the participants' answers. However, for conditions 1 and 10, the participants' responses were not consistent (each condition was randomly repeated 5 times). For example, participant A scored condition 1 with "2, "3", "4", "2", "3" across the 5 repetitions of the test, while participant B scored condition 5 with "2","3", "3", "2", "2". This would indicate that condition 5 receives more robust (consistent) responses than condition 1, as the participant appoints the same score to it more times (in this case, score "2" and "3", instead of score "2", "3" and "4"). Based on this criterion, conditions 2, 5, 6, 8 and 9 were the most robust, as shown in the 3rd column of Table 5. Figure 2.12 shows the distribution of the "robustness percentage" of all conditions, determined by whether a participant's set of (5) responses regarding a condition contained a maximum of 2 different scores (e.g., "2" and "3").

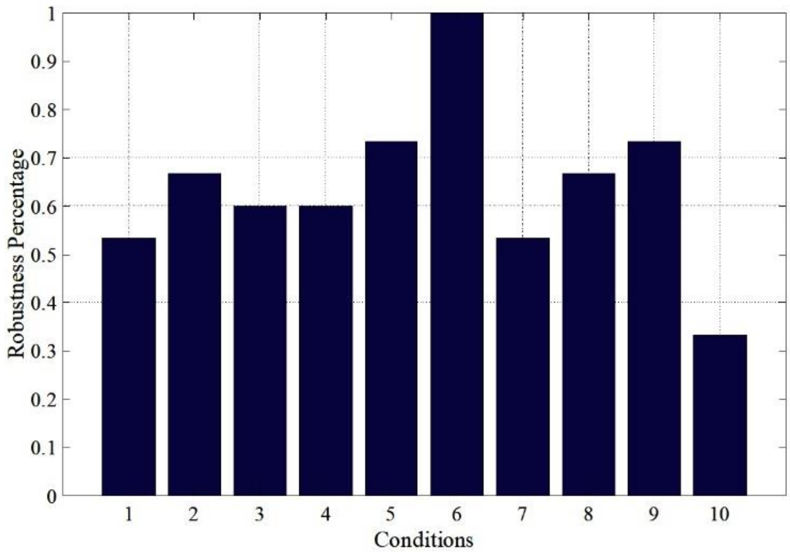

Figure 2.12: Robustness of responses

2.4.3 Path Following and Identification of object hardness in virtual environment

Based on the results of the previous user study and the experimental comparison between various combinations of the two features of the FHD (linear displacement and air volume of the VCP), the "robust" conditions of Table 5 were used to emulate different levels of hardness in a VR environment created in Unity 3D.

Figure 2.11 shows a snapshot of the environment; it includes a path (white) which start and end with 4 red objects placed at random points on the path (the size of each object has no importance in terms of haptic information). This path was the basis of a user study aimed at the evaluation of the FHD and its effectiveness in determining various levels of hardness as well as effectiveness in distinguishing between a safe and a "no-go zone". Testing of the two features simultaneously provides a realistic scenario; for example in a surgical operation where sensory information can be convoluted, and the surgeon must be able to correspond each cutaneous signal to its own stimuli. In total, 14 participants (24–38 years old, ratio of women/men 1:1, ratio of right/left dominant hand 12/2) took part in this study.

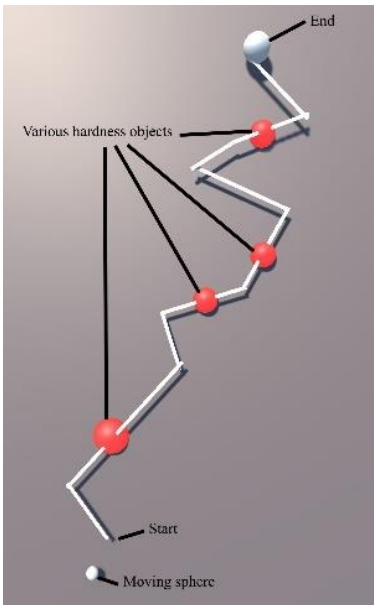

Figure 2.13: Virtual environment created in Unity

Participants were asked to put the FHD on the index finger of their dominant hand, as shown in Fig. 2.9A, and use it to move the small white sphere (bottom part of Fig. 2.13) along the path. They did this by tilting their index finger (pitch) to control the forward/backward movement and pointing in the direction parallel to the sphere's chosen path (yaw). The IMU tracks the change of direction and the virtual sphere moves accordingly. The goal of the task was to move the sphere from start to end as fast and as accurately as possible, while receiving haptic feedback from the FHD. Force feedback is initiated when the small white sphere derails from the path as well as when it touches a red object (lump). The participants also need to discern which 2 of the 4 red lumps are the hardest.

A short "training" session allowed participants to familiarise themselves with navigation in the VR environment following a path (different to the path of the main experiment) and the various hardness levels by interacting with virtual objects. Subsequently, each participant completed 3 sets of a total of 6 tasks in a random sequence. In each of the 6 tasks, the participants experience various levels of haptic feedback when the sphere moves off-path and when it touches the red lumps. The levels of hardness of the red lumps were chosen randomly and are summarised in Table 4. In task 4, the FHD provided no haptic feedback when the sphere derailed from the path or was on the lumps. Furthermore, the area surrounding the path was divided in 3 zones (inner, middle and outer zone), triggering levels of haptic feedback corresponding to increasing hardness as the sphere derails from the path, as shown in Table 6.

Table 6

	Hardness level of red lump				Level of haptic feedback in zones surrounding path			User success rate in detecting the hard red lumps
	1st	2nd	3rd	4th	Inner	Middle	Outer	
Task 1	“2”	“4”	“3”	“4”	“3”	“2”	“1”	83.3%
Task 2	“3”	“5”	“5”	“3”	“5”	“4”	“3”	80%
Task 3	“3”	“2”	“3”	“2”	“1”	“1”	“1”	78.6%
Task 4	No haptic feedback							n/a
Task 5	“5”	“3”	“3”	“5”	“4”	“3”	“2”	90.5%
Task 6	“3”	“3”	“3”	“4”	“2”	“1”	“1”	84.5%

The tests performed with users were initially designed to detect abnormal growth in the tissue. By changing the virtual environment, we can similarly detect ‘holes’ or ruptures in meniscus. Further work is required to test the efficiency of the FHD in the simulated environment, on ‘wet knee’ phantoms, on ex-vivo animals, and will involve orthopaedic surgeons.

3. Force sensing for haptics in RAMIS

Force and tactile sensing at the surgical site is a pre-requisite for haptic feedback. Many attempts have been made in the last 25 years to develop sensorised surgical instruments as a means to detect interaction forces between the instrument and tissue. However, the size of force sensors and incision ports, the sterilisation of tools at high temperatures as well as the disposable nature of surgical tools have so far prevented integration of tissue force/tactile sensing in laparoscopy and RAMIS [25, 26].

3.1 Sensor-less force sensing

Visual estimation of shaft deformation [27], modelling of surgical tool-tissue interaction [28] and the use of motor current [29,30] are examples of sensor-less force estimation algorithms, i.e. sensing methods that do not require sensing hardware at the surgical operating site. Sang et al. modelled the dynamics of a da Vinci robot and, in conjunction with measured motor current, estimated the external force applied at the tip of the surgical tool [8]. Zhao and Nelson created a 3 degrees-of-freedom (DOF) surgical grasper prototype and modelled joint dynamics as individual linear 2nd order systems to estimate external forces via the motor torque/current relationship [30]. These methods require some form of modelling and simplification (e.g. neglecting friction) which can affect the estimation accuracy. Further, the complexity of these algorithms may not allow for the update rates that are required for haptic feedback, thus affecting the system's overall stability and transparency.

SMARTsurg is using an alternative method to force estimation in a RAMIS context, by acquiring the real-time measurement of the instrument motor current. Off-the-shelf force sensors are characterised and then used to determine the correlation between the motor current and the applied force in palpation and grasping, initially with da Vinci forceps but with the view to use this method for our three-fingered instrument that is under development.

3.1.1 Experimental Setup

Two off the shelf force sensors were used for initial experiments in palpation and grasping; a load cell (CZL635, Phidgets, 49 N range) and a capacitive force sensor (SingleTact, 45 N range). These sensors were calibrated and characterised with the use of calibration masses. The characterisation experiments correlated applied load to voltage and were repeated 3 times, with the voltage averaged and standard deviations of 0 and 0.0022 found for the CZL635 load cell and SingleTact sensor respectively. It was found that the CZL635 load cell has a linear relationship between force and voltage with an R^2 value of 1; while the SingleTact sensor has a cubic relationship between force and voltage with an adjusted R^2 of 0.9988. The relationship between applied load and voltage for the two sensors is illustrated in Fig. 3.1.

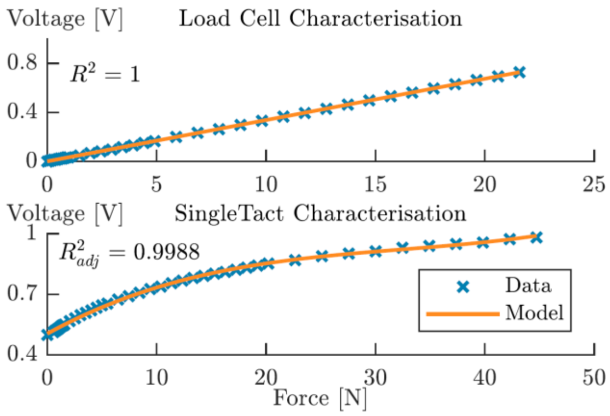

Figure 3.1: Characterisation of the force sensors

Initial experiments in palpation and grasping were conducted using da Vinci forceps. The sensors were used to measure the grasping and palpation forces exerted by the gripper of the forceps as shown in Fig. 3.2a-b. For grasping, two 3D printed (TangoPlus, Stratasys) hemispherical domes were attached to either side of the SingleTact sensor for even distribution of the applied load. The instrument has 4-DOF; pitch, roll, yaw and grasp of the jaws which are controlled by four DC motors in a coupled manner. Only the grasp and yaw of the forceps jaws were actuated for the initial experiments via two Maxon DC motors (3.89mNm, 62:1 reduction). A custom housing was made to attach the gearbox of the instruments to the shafts of the motors, as shown in Fig. 3.2c-d. The shafts of the motors were connected to the gearbox of the instrument via the blue cogs highlighted in Fig. 3.2d, with the pitch and roll kept constant by the red cogs. Palpation was conducted by moving the two motors in the same direction and supplying them with equal magnitude current; whilst grasping was conducted by moving the two motors in opposing directions but supplying them with equal magnitude current.

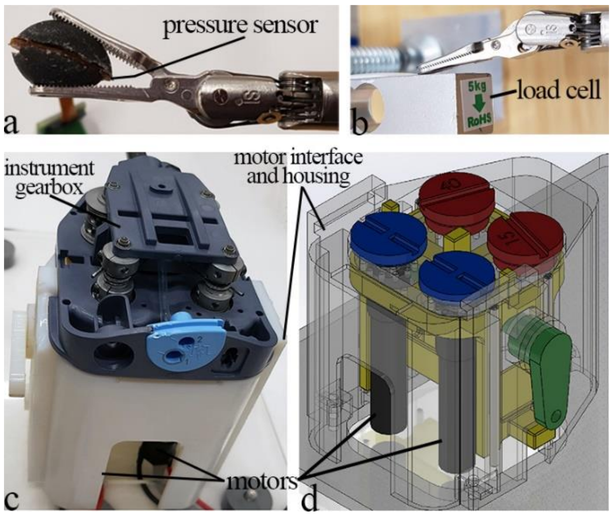

Figure 3.2: da Vinci forceps **a)** grasping the dome-sensor, **b)** applying vertical force to the load cell, **c)-d)** with a custom-made housing for the motors

3.1.2 Preliminary results

The correlation between measured forces in grasping and palpation scenarios, and the current of the motors was found by driving the motors using current control. Sensor readings were taken for every 0.1mA increase of the current between 10-309mA (maximum continuous current of the motors). The experiments were each repeated ten times for both scenarios. The results were then filtered using smoothing splines and averaged with standard deviation of 0.63 (grasping) and 0.12 (palpation). As illustrated in Fig. 3.3, there is a linear relationship between current and force for grasping, while the correlation of palpation force to motor current can be modelled with a cubic polynomial.

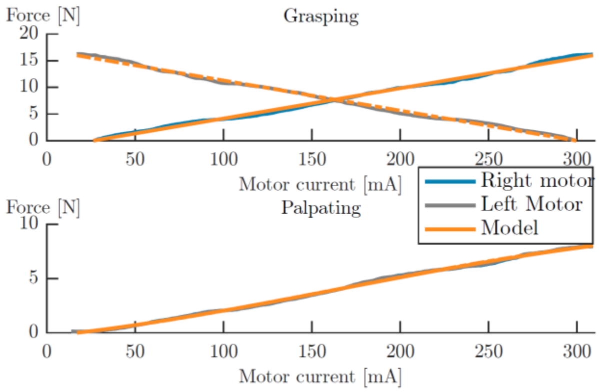

Figure 3.3: Correlation between the current of the motors and forces applied during grasping and palpation by the right and left jaws of the da Vinci forceps

3.1.3 Discussion and future work

The maximum (averaged) forces recorded were 17 N for grasping and 8 N for palpation, which were lower than expected. This was due to friction and the coupling of the instrument's cable-driven system [31] between the mechanisms responsible for the grasping/yaw and those for the roll and pitch. In this experiment, roll and pitch were kept constant (red cogs in Fig. 3.2).

Nevertheless, the results suggest that correlation between motor current and forces exerted by the end-effector can be found for both grasping and palpation. This is highly beneficial in surgical applications where miniaturisation and sterilisation of instruments prevent the attachment of sensors directly to the tips of the surgical tool. Furthermore, the results show that palpation is possible by pushing with the grasper without having to grasp the tissue as previously done in [30], which can be more intuitive for the surgeon.

The initial investigations have shown promise in correlating grasping and palpation forces to motor current. In the future, this work is to be expanded to the three-fingered surgical tool currently under development in the SMARTsurg project. This mechanism will have greater articulation than the da Vinci forceps. As such, a thorough investigation into the correlation between force and motor current using greater numbers of DOF in surgical manoeuvres than what was done in the preliminary investigations will be conducted.

3.2 Force sensing for suturing task

As discussed in Section 2.3, the wrist motion of the surgical instrument is to be controlled via the Virtuose 6D Desktop device. Therefore, the thread pulling forces encountered in a suturing task need to be measured in order to be reflected on the Virtuose 6D Desktop device.

Stages 2 and 3 of the haptic feedback implementation (Section 2.3) consider suturing tasks. In Stage 2, the forces that the shaft exerts on the trocar during the performed task are measured by two SingleTact 10N force sensors that are mounted inside the trocar. In Stage 3, the forces exerted by the shaft whilst suturing will be estimated by a FTSens 6 axis torque and force sensor mounted on the KUKA flange.

In both cases, the forces to be reflected back to the user via the master device will be estimated considering both the measurements from the sensors and the measured flange forces as calculated from the joint torques of the slave arm.

4. Conclusion and future work

The presented work is an accurate reflection of our joint endeavours to understand the surgical needs for haptic feedback and translate them into engineering and computing systems capable of providing required information on the instrument/tissue interaction.

Our achievements have so far created solid foundations of sensing and haptic feedback that reflects sensed forces and pressures in the surgical site.

Our further work will focus on:

1. Integration of sensing and haptic feedback
2. Development of the three-fingered surgical instrument and implementation of sensorless force estimation for haptic feedback
3. Tests in laboratory environment with lay users and surgeons using phantoms
4. Tests on ex-vivo animal samples with surgeons
5. Optimisation and refinement of the design and haptic feedback control

HAPTION Virtuose 6D Desktop

The Virtuose 6D Desktop is a haptic device specifically designed for bidirectional interactivity with virtual 3D application. It provides 6 degrees-of-freedom (DOF) with force-feedback.

Its workspace and its small overall dimensions intend it for a use on individual workstations, equipped with a standard monitor.

Technicals Characteristics

The main characteristics of the Virtuose 6D Desktop are :

- 6 degrees of freedom position feedback
- 6 degrees of freedom active force-feedback
- Operational workspace corresponding to the movements of the lower arm pivoting around the elbow: 521 x 370 x 400 mm and 270° x 120° x 250°
- Continuous translation force of 3 N (Maximum 10N)
- Continuous rotation torque of 0.2 Nm (Maximum 0.8 Nm)
- Passive weight balancing with springs
- Lightweight, no specific equipment needed for transport
- Support of both impedance (force) and admittance (position) control
- Development kit (API) available for Microsoft Windows and Linux (32 and 64 bits)
- Communication through Ethernet/UDP
- Tool fixation through a standard M8 connector for easy customization

Virtuose 6D Desktop

Workspace

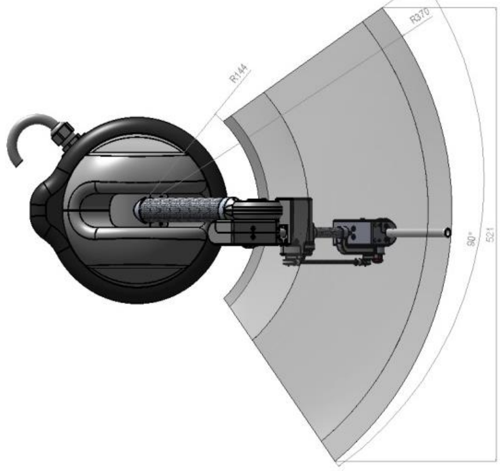

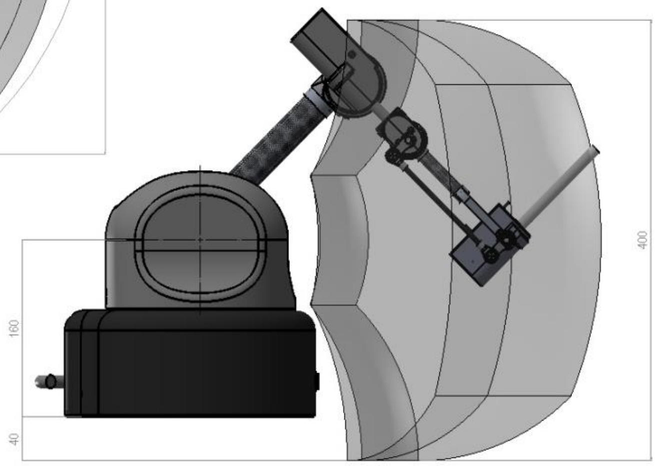

The Virtuose 6D Desktop is composed of three articulated branches, attached in serial to the grasping tool, which give a 6 degrees-of-freedom kinematics, with forcefeedback available in all degrees-of-freedom. The structure of the Virtuose 6D Desktop makes it possible to work in a volume of 521 x 370 x 400 mm. The resolution in position is of 0.01 mm.

Characteristics

Number of motors	6
Type of motors	DC
Output power of the motors	60W in 48V
Power supply	100-240 VAC one-phase
Power consumption	Less than 200W
Translation force: Peak, Continuous	3 N, 10 N
Rotation force: Peak, Continuous	0.2 Nm, 0.8 Nm
Maximum control stiffness (translation)	1000 N/m
Maximum control stiffness (rotation)	4Nm/rad
Apparent inertia	350 g
Weight of the haptic arm	3.6 kg
Weight of the power supply	2.1 kg

HAPTION S.A.
Atelier relais ZA Route de Laval – 53210 SOULGE SUR OUETTE – France
tel. +33(0)2 43 64 51 20
fax. +33(0)2 43 64 51 21
e-mail. contact@haption.com
http://www.haption.com

Technical data

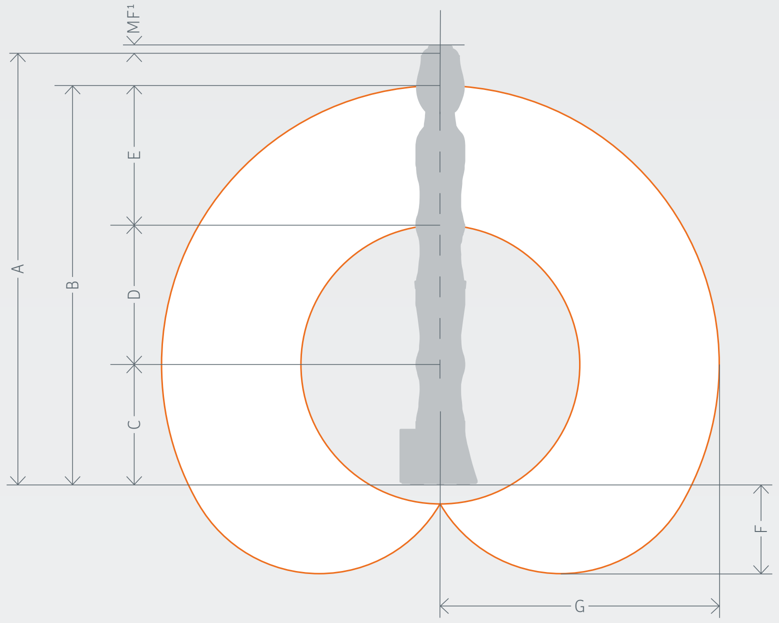

¹ dependent on the media flange option

Workspace	Dimensions A	Dimensions B	Dimensions C	Dimensions D	Dimensions E	Dimensions F	Dimensions G	Volume
LBR iiwa 7 R800	1,266 mm	1,140 mm	340 mm	400 mm	400 mm	260 mm	800 mm	1.7 m³
LBR iiwa 14 R820	1,306 mm	1,180 mm	360 mm	420 mm	400 mm	255 mm	820 mm	1.8 m³

LBR iiwa	LBR iiwa 7 R800	LBR iiwa 14 R820
Rated payload	7 kg	14 kg
Number of axes	7	7
Wrist variant	In-line wrist	In-line wrist
Mounting flange A7	DIN ISO 9409-1-A50	DIN ISO 9409-1-A50
Installation position	any	any
Positioning accuracy (ISO 9283)	± 0.1 mm	± 0.1 mm
Axis-specific torque accuracy	± 2 %	± 2 %
Weight	23.9 kg	29.9 kg
Protection rating	IP 54	IP 54

Axis data / Range of motion		LBR iiwa 7 kg Maximum torque	LBR iiwa 7 kg Maximum velocity	LBR iiwa 14 kg Maximum torque	LBR iiwa 14 kg Maximum velocity
Axis 1 (A1)	± 170°	176 Nm	98°/s	320 Nm	85°/s
Axis 2 (A2)	± 120°	176 Nm	98°/s	320 Nm	85°/s
Axis 3 (A3)	± 170°	110 Nm	100°/s	176 Nm	100°/s
Axis 4 (A4)	± 120°	110 Nm	130°/s	176 Nm	75°/s
Axis 5 (A5)	± 170°	110 Nm	140°/s	110 Nm	130°/s
Axis 6 (A6)	± 120°	40 Nm	180°/s	40 Nm	135°/s
Axis 7 (A7)	± 175°	40 Nm	180°/s	40 Nm	135°/s

Programmable Cartesian stiffness		
Min. (X, Y, Z)	0.0 N/m	0.0 N/m
Max. (X, Y, Z)	5,000 N/m	5,000 N/m
Min. (A, B, C)	0.0 N/rad	0.0 N/rad
Max. (A, B, C)	300 Nm/rad	300 Nm/rad

KUKA Sunrise Cabinet	
Processor	Quad-core processor
Hard drive	SSD
Interfaces	USB, EtherNet, DVI-I
Protection rating	IP20
Dimensions (D x W x H)	500 mm x 483 mm x 190 mm
Weight	23 kg

Power supply connection	
Rated supply voltage	AC 110 V to 230 V
Permissible tolerance of rated voltage	± 10 %
Mains frequency	50 Hz ± 1 Hz or 60 Hz ± 1 Hz
Mains-side fusing	2 x 16 A slow-blowing

30,000 operating hours

Media flange options

The energy supply system for the external components of the LBR iiwa is hidden in the kinematic structure of the robot. Two energy supply systems are available:

Pneumatic
2 x air (diameter 4.0 mm)
2 x electrical (1.0 mm²)
1 x EtherNet-capable cable

Electrical
3 x twisted two-wire cables (AWG28)
4 x electrical (1.0 mm²)
1 x EtherNet-capable cable

All media flanges have a hole pattern conforming to DIN ISO 9409-1-50-7-M6. The following media flanges are available:

Selection matrix for media flanges	Basic flange	Media flange electrical	Media flange pneumatic	Media flange IO electrical	Media flange IO pneumatic	Media flange Touch electrical	Media flange Touch pneumatic	Media flange IO valve pneumatic	Media flange Inside electrical	Media flange Inside pneumatic
Interface for CAT5 and analog signals (4 pins)		●	●						●	●
Interface for CAT5 and analog signals (6 pins)		●		●		●			●	
Interface for energy supply system (3 A, 24 V), no external power supply required				●	●	●	●	●		
Interface for energy supply system (max. 4 A, max. 60 V) with external power supply				●		●				
Interface for energy supply system (max. 5 A, max. 60 V) with external power supply		●							●	
Interface for energy supply system (max. 8 A, max. 30 V) with external power supply			●							
Interface for energy supply system (max. 8 A, max. 60 V) with external power supply		●							●	●
Pneumatic interface with 2 compressed air connections			●		●		●			●
EtherCAT connection				●	●	●	●	●		
Configurable inputs and outputs for direct connection of sensors and other electrical components				●	●	●	●	●		
Enabling switch, programmable application switch, programmable visual display (LED)						●	●			
Grip for manual mode						●	●			
Intelligent pneumatic interface: 2 integrated bistable valves and 1 additional air connection								●		

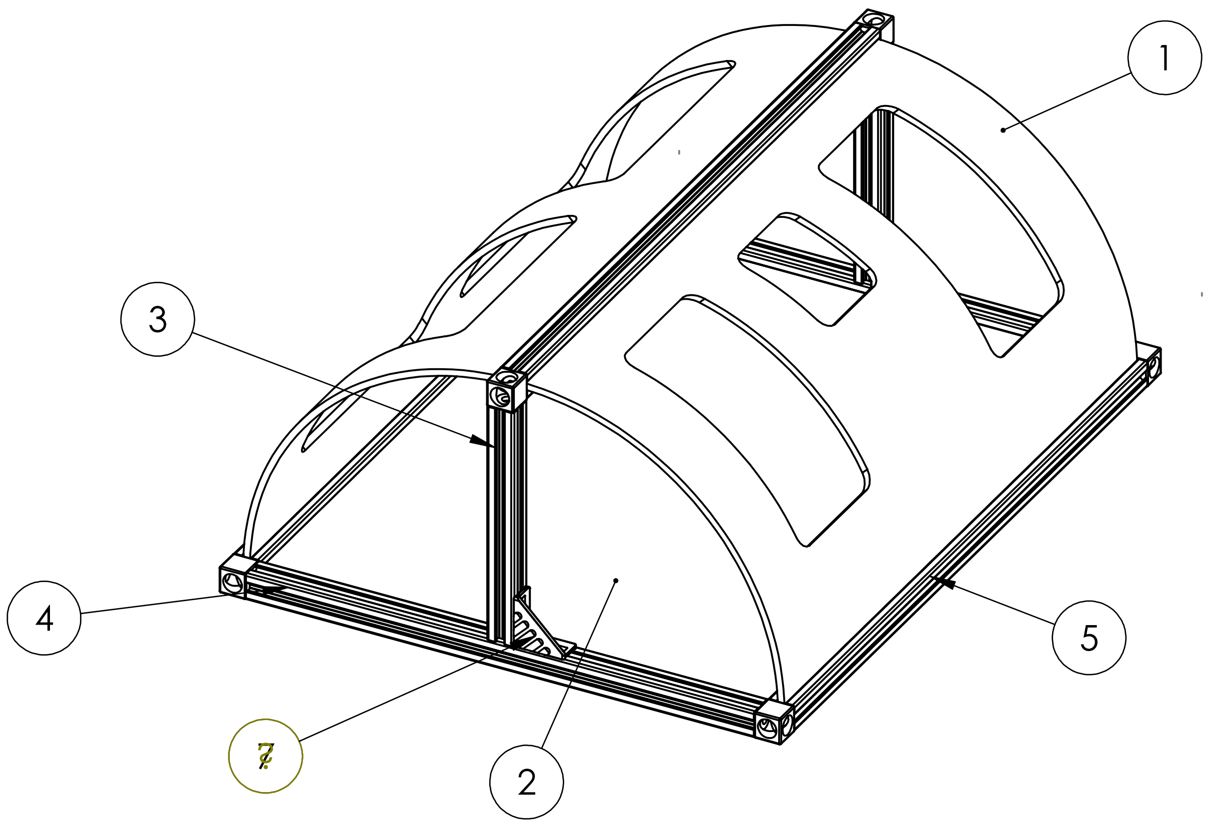

ITEM NO.	PART NUMBER	QTY.
1	400mm acrylic tube quarter section	2
2	6mm perspex sheet	1
3	180 mm (20 x 20 6mm 4x Slot)	2
4	380 mm (20 x 20 6mm 4x Slot)	2
5	500mm (20 x 20 6mm 4x Slot)	3
6	20 x 40 Corner	2
7	20x20 2 Way Cube Connector	6

Note: The slots in the acrylic tube are arbitrary and not final

TITLE Phantom	A4
	mm
SCALE:1:5	SHEET 1 OF 1

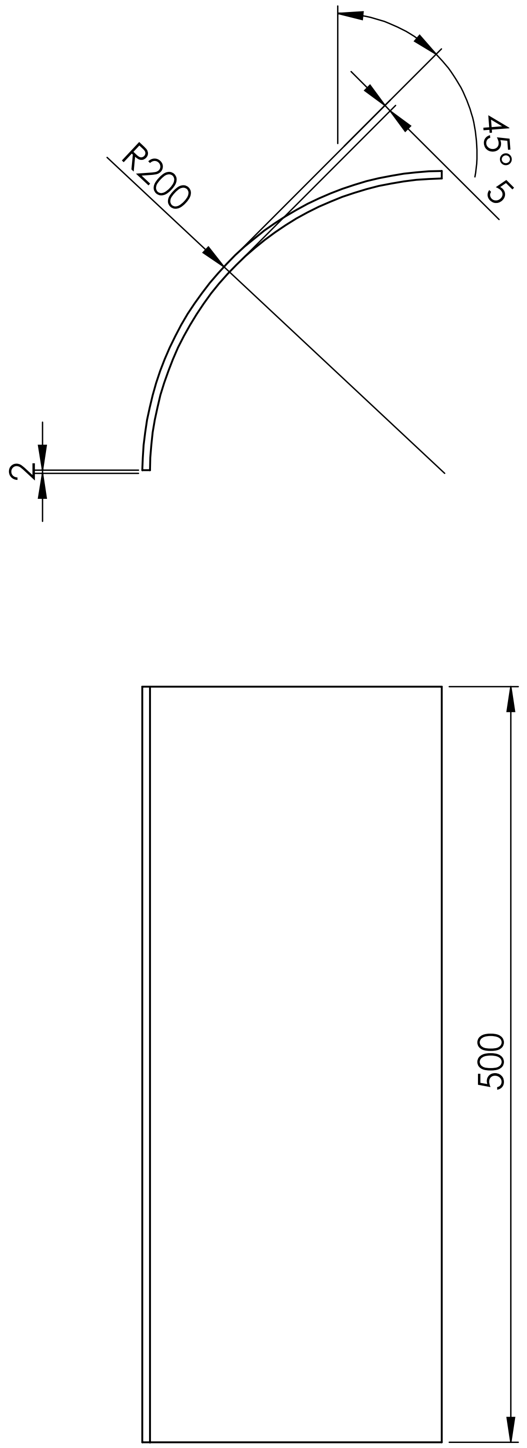

TITLE 400 mm acrylic tube quarter section	A4
	mm
SCALE:1:5	SHEET 2 OF 6

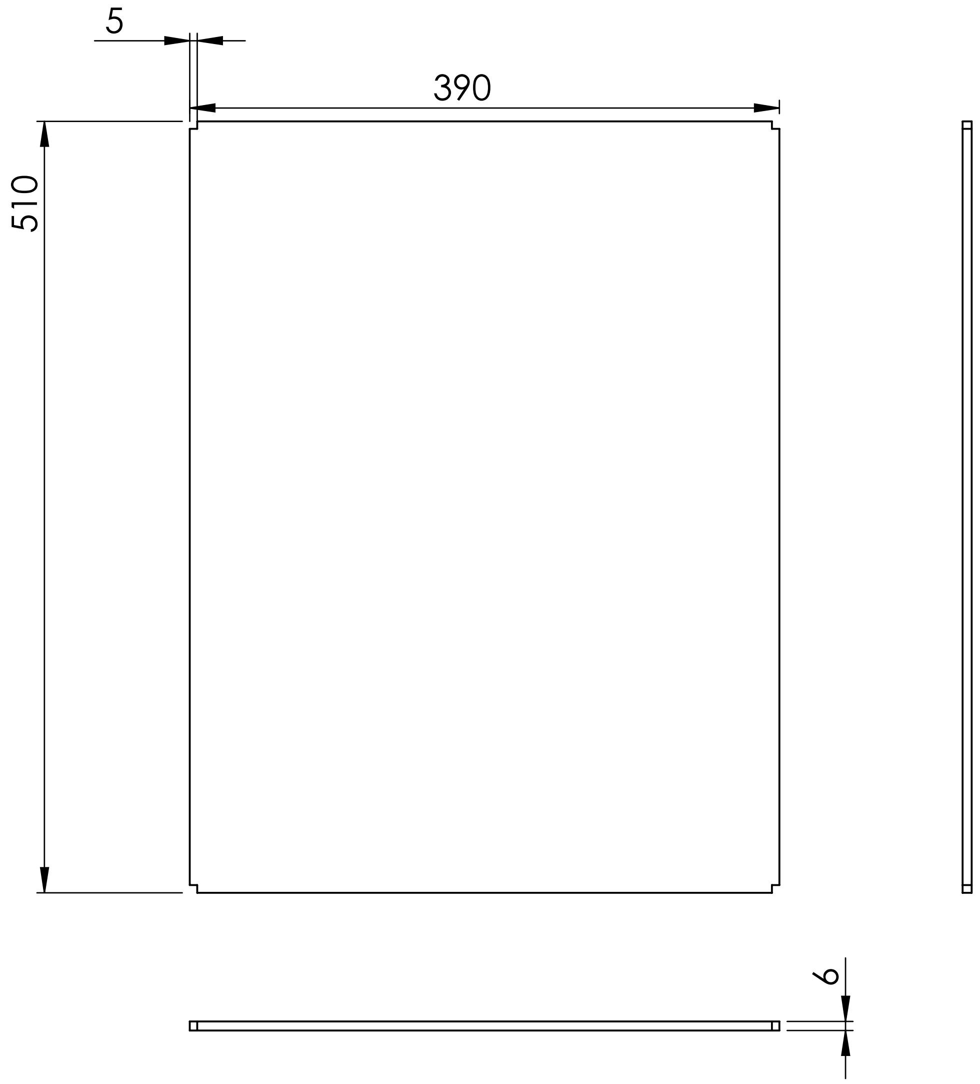

TITLE	6mm Perspex Sheet	A4
		mm
SCALE:1:5	SHEET 3 OF 6	

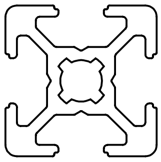

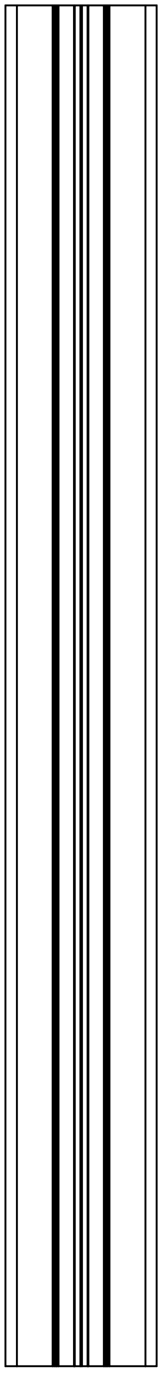

TITLE 20 x 20 6mm 4x Slot (various lengths)	A4 mm
SCALE:1:1	SHEET 4 OF 6

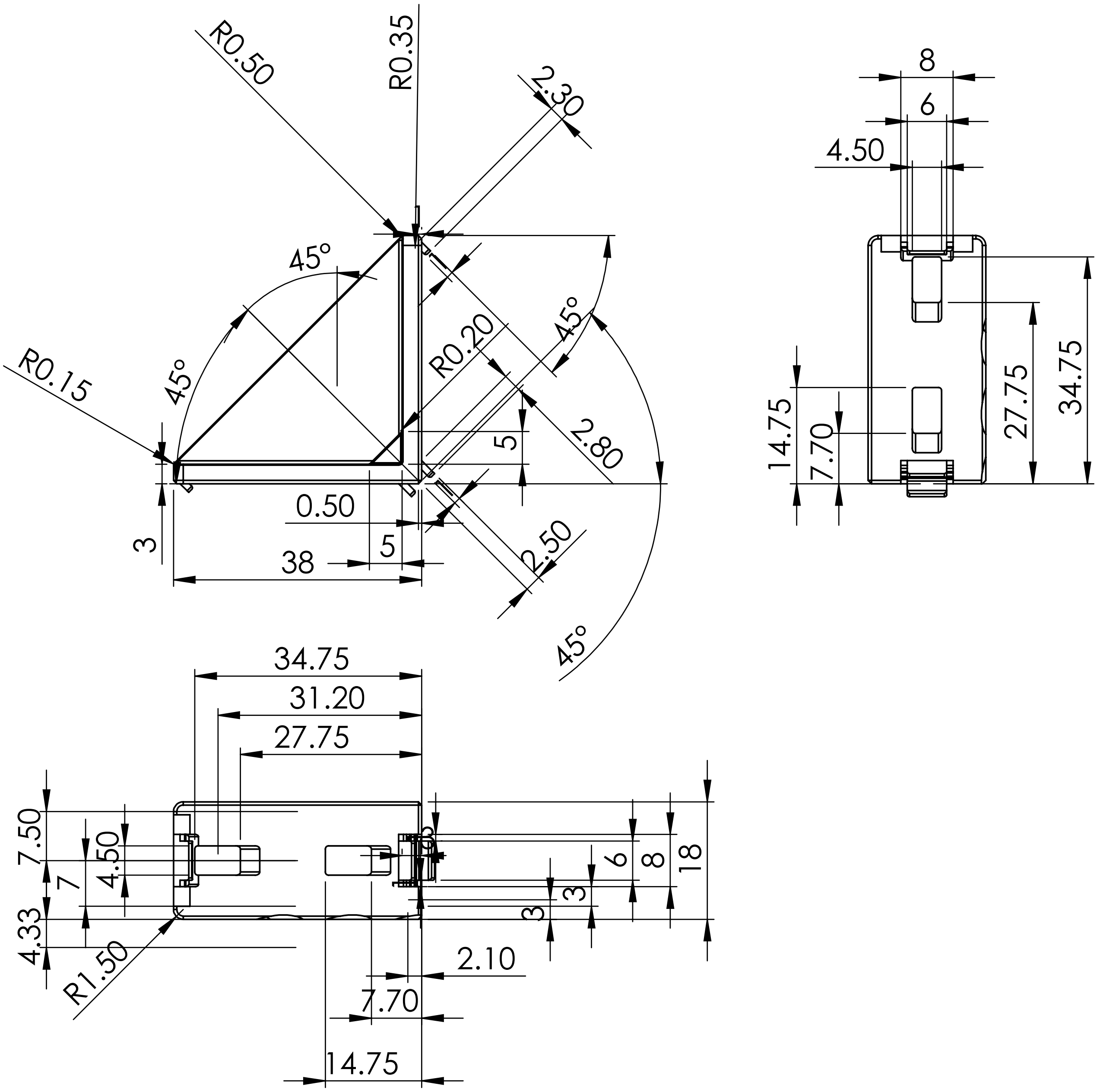

TITLE 20 x 40 Corner	A4
	mm
SCALE:1:5	SHEET 5 OF 6

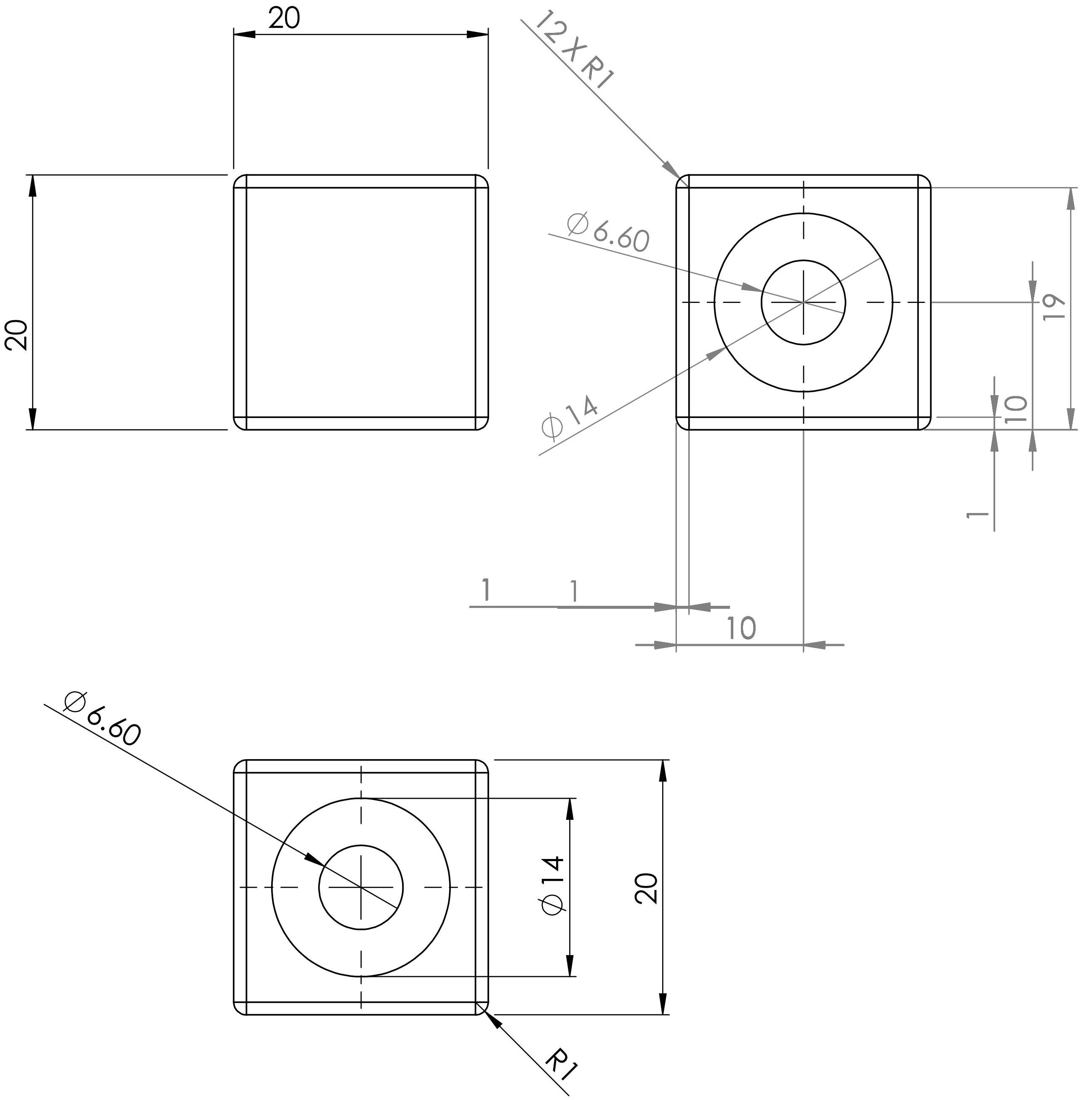

TITLE 20 x 20 2 Way Cube Connector	A4 mm
SCALE:2:1	SHEET 6 OF 6

References

1. A.M. Okamura, "Haptic feedback in robot-assisted minimally invasive surgery", Current Opinion in Urology, vol. 19, no. 1, pp. 102-107, 2009.

2. H. Yamanaka, K. Makiyama, K. Osaka, M. Nagasaka, M. Ogata, T. Yamada and Y. Kubota, ‘Measurement of the physical properties during laparoscopic surgery performed on pigs by using forceps with pressure sensors’, Advances in Urology, vol. 1, pp. 1-10, 2015.

3. J. Barrie, D. G. Jayne, A. Neville, L. Hunter, A. J. Hood and P. R. Culmer, `Real-time measurement of the tool-tissue interaction in minimally invasive abdominal surgery: The first step to developing the next generation of smart laparoscopic instruments', Surgical Innovation, vol. 23, no. 5, pp. 463-468, 2016.

4. J. Barrie, L. Russell, A. J. Hood, D. G. Jayne, A. Neville and P. R. Culmer,`An in vivo analysis of safe laparoscopic grasping thresholds for colorectal surgery', Surgical Endoscopy, 2018.

5. C.R. Wottawa, B. Genovese, B. N. Nowroozi, S. D. Hart, J. W. Bisley, W. S. Grundfest, and E. P. Dutson, `Evaluating tactile feedback in robotic surgery for potential clinical application using an animal model', Surgical Endoscopy, vol. 30, no. 8, pp. 3198-3209, 2016.

6. C. C. J. Alleblas, M. P. H. Vleugels, S. F. P. J. Coppus, and T. E. Nieboer, `The effects of laparoscopic graspers with enhanced haptic feedback on applied forces: a randomized comparison with conventional graspers', Surgical Endoscopy, vol. 31, no. 12, pp. 5411-5417, 2017.

7. A. Talasaz and R.V. Patel, ‘Integration of force reflection with tactile sensing for minimally invasive robotics-assisted tumor localization’, IEEE Transactions on Haptics, vol. 6, no. 2, 2013.

8. J.C. Gwilliam, M. Mahvash, B. Vagvolgyi, A. Vacharat, D.D. Yuh and A.M. Okamura, ‘Effects of haptic and graphical force feedback on teleoperation palpation’, in IEEE International Conference on Robotics and Automation, 2009, pp. 677-682.

9. A.M. Okamura, ‘Methods for haptic feedback in teleoperated robot-assisted surgery’, The Industrial Robot, vol. 31, no. 6, pp. 499-508, 2004.

10. M. Kitigawa, A.M. Okamura, B.T. Bethea, V.L. Gott and W.A. Baumgartner, ‘Analysis of suture manipulation forces for teleoperation with force feedback’, in International

Conference on Medical Image Computing and Computer-Assisted intervention, 2002, pp.155-162.

11. M. Tavakoli, R.V. Patel and M. Moallem, ‘Robotic suturing forces in the presence of haptic feedback and sensory substitution’, IEEE Conference on Control Application, 2005, pp. 1-6.

12. A. Talasaz, A.L. Trejos and R.V. Patel, ‘The role of direct and visual force feedback in suturing using a 7-DOF dual-arm teleoperated system’, IEEE Transactions on Haptics, vol. 10, no.2, 2017.

13. A. Garcia Ruiz, M. Gagner, J.H. Miller, C.P. Steiner & J.F. Hahn, ‘Manual vs robotically assisted laparoscopic surgery in the performance of basic manipulation and suturing tasks’, Archives of Surgery, vol. 133, no. 9, pp. 57– 61, 1998.

14. J. Ruurda, I. A. M. J. Broeders, B. Pulles, F. Kappelhof, & C. van der Werken, ‘Manual robot assisted endoscopic suturing: time-action analysis in an experimental model’, Surgical Endoscopy, vol. 18, no. 8, pp. 1249-1252, 2004.

15. T.P. Kelliher, J. Lenoir, P. Novotny, and H. Scheirich, ‘Open Surgical Simulation (OSS)-A Community Resource’ in Medicine Meets Virtual Reality, 2014, pp. 197-203.

16. A. Tzemanaki, G.A. Al, C. Melhuish and S. Dogramadzi, ‘Design of a Wearable Fingertip Haptic Device for Remote Palpation: Characterisation and Interface with a Virtual Environment’, Frontiers in Robotics and AI, vol 5, 2018.

17. M. Peters, K. Mackenzie, and P. Bryden, ‘Finger length and distal finger extent patterns in humans’, American Journal of Physical Anthropology, vol. 117, no. 3, pp. 209–217, 2002.

18. D. Tsetserukou, K. Sato, and S. Tachi, ‘Exo-interfaces: novel exoskeleton haptic interfaces for virtual reality, augmented sport and rehabilitation’, in Proceedings of the 1st Augmented Human International Conference, 2010.

19. D. Leonardis, M. Solazzi, I. Bortone, and A. Frisoli, (2015), ‘A wearable fingertip haptic device with 3-DOF asymmetric 3-RSR kinematics’, in IEEE World Haptics Conference (WHC), 2015, pp. 388–393.

20. S.B. Schorr and A.M. Okamura, ‘Three-dimensional skin deformation as force substitution: Wearable device design and performance during haptic exploration of virtual environments’, IEEE Transactions on Haptics, vol. 10, no. 3, pp. 418-430, 2017.

21. K. Minamizawa, S. Fukamachi, H. Kajimoto, N. Kawakami, and S. Tachi, (2007), ‘Gravity grabber: wearable haptic display to present virtual mass sensation’, in ACM SIGGRAPH 2007 emerging technologies, p. 8.

22. C. Pacchierotti, A. Tirmizi, and D. Prattichizzo, ‘Improving transparency in teleoperation by means of cutaneous tactile force feedback’, ACM Transactions on Applied Perception, vol. 11, no. 1, pp. 4:1-4:16, 2014.

23. I. M. Koo, K. Jung, J. C. Koo, J.D. Nam, Y. K. Lee, and H. R. Choi, ‘Development of soft-actuator-based wearable tactile display’, IEEE Transactions on Robotics, vol. 24, no. 3, pp. 549-558, 2008.

24. G. Frediani, D. Mazzei, D. E. De Rossi and F. Carpi, ‘Wearable wireless tactile display for virtual interactions with soft bodies’, Frontiers in Bioengineering and Biotechnology, vol. 2, 2014.

25. P. Puangmali, K. Althoefer, L. D. Seneviratne, D. Murphy, and P. Dasgupta, ‘State-of-the-art in force and tactile sensing for minimally invasive surgery’, IEEE Sensors, vol. 8, no. 4, pp. 371-381, 2008.

26. A. J. Spiers, H. J. Thompson, and A. G. Pipe, ‘Investigating remote sensor placement for practical haptic sensing with EndoWrist surgical tools’, in IEEE World Haptics Conference, 2015, pp. 152-157.

27. Q. J Lindsey, N. A Tenenholtz, D. Lee, and K. J Kuchenbecker, ‘Image-enabled force feedback for robotic teleoperation of a flexible surgical tool’, in Proceedings of the IASTED International Conference on Robotics and Applications, 2009.

28. A. M. Okamura, C. Simone, and M. D. O’Leary, ‘Force modelling for needle insertion into soft tissue’, IEEE Transactions on Biomedical Engineering, vol. 51, no. 10, pp. 1707-1716, 2004.

29. H. Sang, J. Yun, R. Monfaredi, E. Wilson, et al., "External force estimation and implementation in robotically assisted minimally invasive surgery", The International Journal of Medical Robotics and Computer Assisted Surgery, vol. 13, no. 2, 2017.

30. B. Zhao and C. Nelson, ‘Sensorless force sensing for minimally invasive surgery’, Journal of Medical Devices, vol. 9, no. 4, pp. 041012:1-14, 2015.

31. C. Y. Kim, M. C. Lee, R. B. Wicker, and S.-M. Yoon, ‘Dynamic modeling of coupled tendon-driven system for surgical robot instrument’, International Journal of Precision Engineering and Manufacturing, vol. 15, no. 10, pp. 2077-2084, 2014.